Adsorption and Desorption of PEO−PPO−PEO Triblock Copolymers on a Self-Assembled Hydrophobic Surface

Pietro Brandani*,† and Pieter Stroeve*

Department of Chemical Engineering and Materials Science, University of California, Davis, One Shields Avenue, Davis, California 95616

Received February 28, 2003; Revised Manuscript Received August 14, 2003

ABSTRACT: We report on the adsorption from solution of a family of triblock copolymers, copoly(ethylene oxide−propylene oxide−ethylene oxide) (PEO−PPO−PEO), on a gold surface modified by a methyl-terminated, self-assembled monolayer (SAM) of a long-chain alkanethiol ($CH_3(CH_2)_{10}SH$). We employed a surface plasmon resonance (SPR) technique to determine polymer-adsorbed amounts. We also performed atomic force microscopy (AFM) in the liquid environment on a selected number of cases to discern the morphology of the copolymer-coated surfaces. This study shows that the adsorbed amounts go through a maximum near the critical micelle concentration (cmc) and that the process is only partially reversible. Trends in the adsorbed amounts with varying relative composition of the copolymer blocks are consistent with scaling law predictions for the adsorption of block copolymers from selective solvents. AFM imaging shows micellar aggregates at the surface for a copolymer with higher relative hydrophobic content. In contrast, for a copolymer with higher hydrophilic content, we observe a uniform, monolayer-like morphology. In both cases, cycling of the force on the AFM tip reveals the presence of a polymer brush.

Introduction

Copolymers that have constituent blocks with different affinities for their surroundings exhibit amphiphilic properties; that is, they, like the more conventional surfactants, self-organize or self-assemble at interfaces and in solution in order to minimize contact between less compatible parts. This behavior can be exploited to change the properties of surfaces and to enhance solubilities in solution. Lately, the emphasis has shifted toward the design and creation of functional, adsorption-driven, self-assembled nanostructures.[9,29,33] Understanding the modality of interactions between polymers and surfaces is fundamental in the pursuit of this task. We have focused our attention on a family of triblock copolymers, comprised of ethylene oxide (EO) and propylene oxide (PO) blocks in the form PEO_nPPO_m-PEO_n (we shall use the simplified notation $E_nP_mE_n$ for the remainder of the paper) and known by their commercial trade name of Pluronics, adsorbing on a model hydrophobic surface consisting of a self-assembled monolayer (SAM) of a methyl-terminated alkanethiolate on gold. At room temperature the EO blocks and the PO blocks that make up the copolymers are hydrophilic and hydrophobic, respectively, making these compounds belong to the class of nonionic surface-active agents.

We have opted to probe our surfaces with a surface plasmon resonance spectroscopy (SPR) apparatus. SPR allows in-situ, nondestructive sampling of the deposition process in its native environment. Similarly, the species of interest retain their native physical characteristics since they do not need to include or be modified to include additions to their structure such as light-absorbing chromophores or radioactive labeling moieties. We have also examined the structure of the deposited layers of a selected number of systems by atomic force microscopy (AFM).

Green et al. have previously reported on the subject of PEO−PPO−PEO adsorption on a planar hydrophobic surface.[19] However, the absence of quantitative analysis of the SPR response curves only allowed the authors to make qualitative statements about the system.

The aim of this study is to investigate the influence of copolymer structure on the kinetics of adsorption and desorption of PEO−PPO−PEO triblock copolymers on model hydrophobic surfaces and provide an account of the adsorption behavior on a quantitative basis. The contents of the paper are as follows: we first present the results of adsorbed amount measures for the static systems. We will show that the adsorption isotherms cannot be described by a Langmuir-type expression over the full range of concentrations given that a maximum in the adsorbed amount is observed in the vicinity of the critical micelle concentration (cmc). Likewise, desorption data show that the process is only partially reversible. We examine our results in the context of scaling law theory to show that they are consistent with a brush configuration at the surface. We, then, use AFM to look at the morphology of a select number of polymer-coated surfaces. We confirm the distinct nature of the adsorption processes for P103 ($E_{17}P_{60}E_{17}$, a more hydrophobic species) and P105 ($E_{37}P_{56}E_{37}$, a more hydrophilic species) by observing differences in the types of structures present at the surface following adsorption.

Experimental Section

Materials. The Pluronic surfactants P123 ($E_{19}P_{69}E_{19}$), P103 ($E_{17}P_{60}E_{17}$), P104 ($E_{27}P_{61}E_{27}$), P105 ($E_{37}P_{56}E_{37}$), and F108 ($E_{132}P_{50}E_{132}$) were a gift from BASF Corp. Deionized (DI) water (18.2 MΩ cm) from a NanoPure system (Barnstead, IA) was used to prepare the polymer solutions and to run the water rinsing steps in the experiments. All solvents and chemicals were of analytical grade. The ethanol used in thiol solution preparation was absolute 200 proof (Gold Shield Chemical Co.,

† Present address: Center for Biophotonics Science & Technology, University of California, Davis, 4800 2nd St, Suite 2600, Sacramento, CA 95817.

* To whom correspondence should be addressed: Tel 530-752-8778, Fax 530-752-1031, e-mail pstroeve@ucdavis.edu; Tel 530-754-7212, Fax 530-752-2444, e-mail pbrandani@ucdavis.edu.

10.1021/ma0342675 CCC: $25.00
Published on Web 11/14/2003

Riverside, CA). Undecanethiol used for the formation of monolayers on gold was purchased from Aldrich-Sigma.

Preparation of Gold Slides. We have used high refractive index LaFSN9 glass slides (Schott, Germany) as substrates for SPR experiments and mica sheets as substrates for AFM. Gold of 99.999% purity was used to coat the glass substrates by sputtering. About 50 nm of gold was deposited on the glass slides by heating a gold target in a crucible with an electron beam at a pressure below 5×10^{-6} Torr, with a gold deposition rate of 0.2 Å/s. Finally, the gold slides were annealed at 650 °C for 30 s to minimize the surface roughness of the gold.[22]

Preparation of Thiol Monolayers. When gold is exposed to a thiol solution, self-assembled monolayers form spontaneously. Typically thiolate self-assembled monolayers can be modified through syntheses of alkanethiols with varying terminal groups to adjust surface energies and charge.[11] In this study we have used a methyl-terminated SAM to achieve a model hydrophobic surface. Self-assembly of the thiol monolayers was achieved by injecting a 5 mM undecanethiol solution in alcohol into the flow cell containing a freshly prepared gold slide. The solution was allowed to react with the gold for at least 16 h, a time considered to be adequate for SAM formation, and then rinsed with at least 20 mL of ethanol at a flow rate of 5 mL/min and at least 200 mL of water at a flow rate of 10 mL/min to reach complete removal of thiol residue. SPR kinetics experiments showed that more than 99% of undecanethiolate SAM formation was complete within 16 h.

Flow-Cell Apparatus. The undecanethiol-coated gold slides were placed on top of a narrow slit cross-section Teflon flow cell. The cell was lined with a BUNA-N O-ring to provide for a watertight seal. The flow chamber was 14 mm wide and 75 mm long. The gap between the glass slide and the Teflon wall was 0.25 mm. The measurement target was 40 mm from the inlet, and the laser target had a cross-sectional area of about 2 mm^2. The target length to inlet gap ratio is 160, which gives fully developed laminar flow at the measurement location.

Surface Plasmon Resonance Spectroscopy. Surface plasmon resonance spectroscopy is a powerful technique for measurements of thin films in air and a variety of solvents; it results from the interplay of two interfacial phenomena. A beam of light that goes through an interface will be partially reflected and partially transmitted across the interface. In the regime of total internal reflection, the refracted light turns into an evanescent wave with a decay length that is typically on the order of 150−200 nm. Oscillations in the electron cloud at a metal−dielectric interface are called surface plasmons. Upon ensuring that the energy and momentum coupling conditions are satisfied,[25] the electron cloud in the metal can be turned into a resonator driven by p-polarized light in the evanescent wave, resulting in the absorption of energy at the interface. This condition will also be manifested in the appearance of a minimum in the angular spectrum of the intensity of the reflected light. The location of this minimum, the resonance angle, is strongly influenced by changes in the dielectric properties of the medium within the decay length of the evanescent wave. The shift in resonance angle is proportional to the amount of material adsorbed at the interface;[8,34,35] thus, SPR can be used to measure the formation of very thin adlayers (down to ∼1 Å) with very fast sampling times (∼0.1 s). In our experiments, we used the Kretschmann configuration to attain the energy and momentum matching conditions between the incoming light and the surface plasmons at the gold−solution interface. A LaSFN9 prism was placed over a gold-coated LaSFN9 glass slide, and monobromonaphthalene (Bellingham & Stanley Ltd., United Kingdom) was used as a matching fluid. Monochromatic p-polarized light from a 633 nm laser was used as the light source. The intensity of the reflected light was captured by a photodiode whose output was sent to a lock-in amplifier (Stanford Research Systems, Sunnyvale, CA) and on to a PC for data handling and storage. A $\theta-2\theta$ goniometer (Huber GmbH, Germany) acted on by a stepper motor capable of 0.001° increments (Blake Industries, Inc., Scotch Plains, NJ) was used to perform scans of the intensity of the reflected light as a function of the incident angle. The SPR curves (reflectivity vs internal angle) were modeled using the characteristic matrix formalism for homogeneous stratified dielectric media.[6,20] A fitting procedure was used in which refractive indices for all layers as well as thicknesses for the inner layers were fixed and the thickness of the last deposited layer calculated to give the least-squares match for the experimental SPR curves. All measurements were performed at room temperature.

Polymer Excess Surface Concentration. Assuming changes in index of refraction are linear with respect to changes in bulk concentration of the solute, one can use the following relation to determine the excess surface concentration of the adsorbed species:[12]

$$\Gamma = \frac{d_f(n_f - n_s)}{dn/dc}$$

where Γ is the block copolymer excess surface concentration (μmol/m^2), d_f is the film thickness (nm), dn/dc (M^{-1}) is the incremental change in the refractive index of solution with the increase in surfactant concentration, n_f is the index of refraction of the polymer film, and n_s is the refractive index of pure solvent, in our case water. The adlayer thickness d_f calculated by the SPR model is strongly dependent on the choice of film refractive index n_f; however, the optical thickness (i.e., the product in the numerator of eq 1) and consequently the adsorbed amount are nearly invariant.[13,36]

Refractive Index Measurements. Refractive index measurements of ethanol, ultrapure water, and aqueous Pluronic solutions were made on an Abbe 60 refractometer (Bellingham & Stanley Ltd., England) using a sodium spectral lamp as the light source ($\lambda = 589.3$ nm). Refractive index of polymer varied linearly with concentration in the range used for this study. Values of the refractive index gradient dn/dc at 25 °C observed for P123, P103, P104, P105, and F108 were 0.13, 0.13, 0.13, 0.14, and 0.12 (±2%), respectively.

Atomic Force Microscopy. The surfaces were imaged with a Nanoscope III (Digital Instruments, Santa Barbara, CA) AFM apparatus in contact mode. An AFM liquid cell (Digital Instruments, Santa Barbara, CA) was utilized to retain the solutions that were injected through plastic tubing. A typical experiment consisted in obtaining first a scan in deionized water, then passing the polymer solution, waiting approximately 20 min to achieve equilibrium conditions, and then performing a scan of the same general area. (Thermal drift and mechanical coupling of the cell and the stage prevented us from scanning the exact same location.) The scans were typically done at rates between 4 and 12 Hz. Feedback gains were set at 1 for the proportional gain and 2 for the integral gain. Set point voltage was varied until soft contact imaging conditions were achieved (see Results and Discussion section for further details). The images were obtained using a gold-coated silicon nitride cantilever with a nominal force constant of 0.05 N m^{-1}. Tilt and bow corrections were applied with the flattening function, but no filtering was otherwise used to process or modify the images.

Results and Discussion

For the investigation we selected a series of Pluronics P123, P103, P104, P105, and F108 on a SAM formed from the deposition of undecanethiol on a gold surface (Table 1). The last four elements in this series have an increasing content of the hydrophilic PEO block and an average content of 57 PO units per PPO block, while the first two have similar EO/PO ratio (EO/PO ∼ 0.56) but differing number of PO units in the PPO block: 69 vs 60 (Figure 1 and Table 1).

Adsorption Isotherms. The adsorption isotherms over the full range studied are presented in Figure 2.

The value of 2.5 mg/m^2 for F108 at $C_b = 0.045$ g/dL (0.01cmc) is comparable with the value 0.88 mg/m^2 at

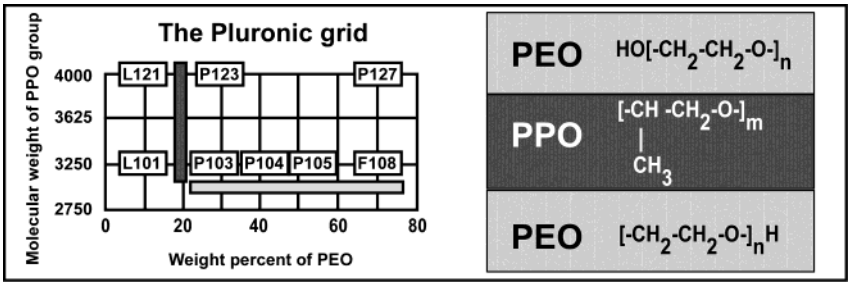

Figure 1. Characteristic grid for the identification of Pluronics: compounds on the same row have the same amount of PO, and compounds in the same column have similar EO/PO.

Table 1. Properties of Pluronics Selected for This Study

polymer	MW	m = no. of PO	n = no. of EO	cmc [μM][a]
P123	5750	69	2 × 19	30
P103	4950	60	2 × 17	168
P104	5900	61	2 × 27	530
P105	6500	56	2 × 37	385
F108	14600	50	2 × 132	3078

[a] Interpolated cmc data at $T = 25$ °C from Alexandridis et al.[2]

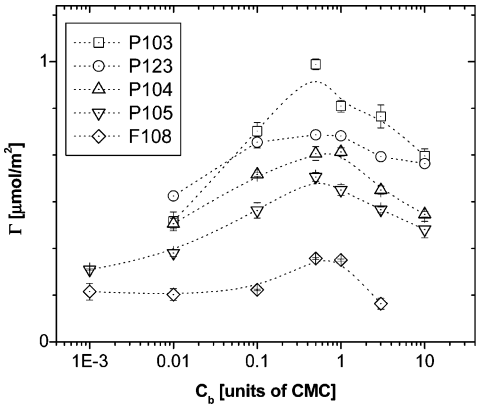

Figure 2. A log−linear graph of the adsorption isotherms for Pluronics P103 ($E_{17}P_{60}E_{17}$), P123 ($E_{19}P_{69}E_{19}$), P104 ($E_{27}P_{61}E_{27}$), P105 ($E_{37}P_{56}E_{37}$), and F108 ($E_{132}P_{50}E_{132}$).

$C_b = 0.02$ g/dL reported by Kayes and Rawlins[23] for adsorption on a polystyrene latex. The prominent features of the data in Figure 3 are that they show maxima in the vicinity of the cmc. As shown in the work of Eskilsson and Tiberg,[17] the decrease observed at the higher concentrations could be due to an artifact of the optical layer modeling used, if a depletion layer is present near the surface. However, in our case we were able to discount this hypothesis by observing that the shift in the SPR critical angle of total internal reflection, which practically depends only on the indices of refraction of the semiinfinite media in our optical layer model, is consistent with changes of the index of refraction for the solution near the surface assuming that the region is at the full bulk concentration. The occurrence of non-Langmuirian-type behavior for Pluronics or similar systems has already been seen in the past.[3,16−18,28] These effects are generally attributed to polydispersity, with the propensity of longer chain polymers to replace shorter chain ones at higher concentrations.[10] In fact, it has been reported that these polymers have a bimodal distribution with an additional lower molecular weight and more hydrophobic fraction.[30] On the other hand, the maxima could be due to a crossover in adsorption mechanism.[28] As the adsorption rates increase with concentration and the deposition is partially irreversible, the system could reach a kinetically induced metastable equilibrium with progressively less efficient packing at the surface.

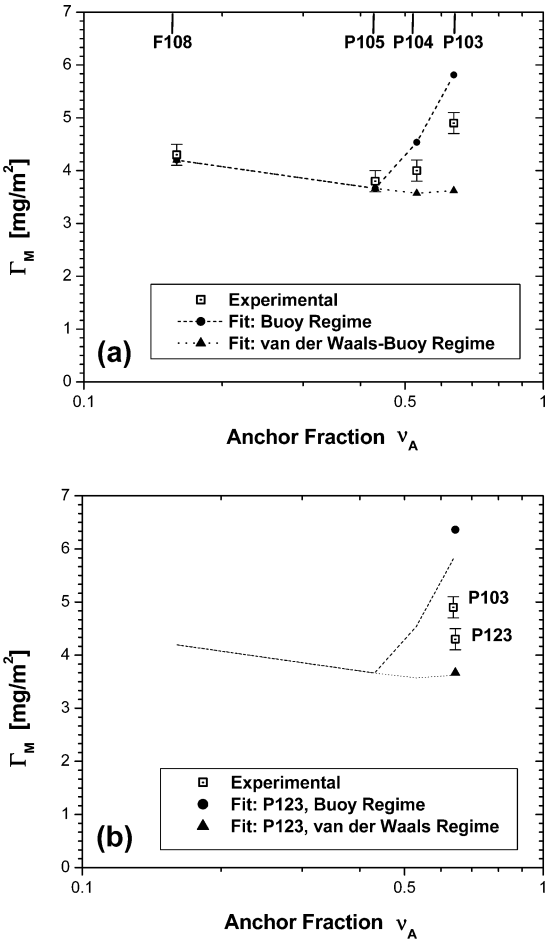

Figure 3. (a) A log−linear graph of the adsorbed amount (mass concentrations) vs the anchor fraction for P103 ($E_{17}P_{60}E_{17}$), P104 ($E_{27}P_{61}E_{27}$), P105 ($E_{37}P_{56}E_{37}$), and F108 ($E_{132}P_{50}E_{132}$). (b) A log−linear graph of the adsorbed amount (mass concentrations) vs the anchor fraction for P123 ($E_{19}P_{69}E_{19}$). Filled circles are the results of the fit for the buoy-dominated regime, and the filled triangles the results of the fit for the van der Waals−buoy regime. The empty squares represent the experimental data points. Lines are included as a guide for the eye.

We can compare the extent of surface coverage at saturation for our solid−liquid system with the data reported in the work of Alexandridis et al.[1] for the same PEO−PPO−PEO species at an air−water interface. Pluronics exhibit tighter packing (about 3-fold, see Table 2) at the air−water interface.

The difference in packing is likely due to the higher configurational entropic penalty sustained by the polymers at a hard wall compared to the more diffuse air−water interface.

Table 2. Comparison of Molecular Areas of the Polymer (Σ_p) at Maximum Surface Coverage between Solution/Methyl-Terminated Solid Interface (Our Experiments) and Solution/Air Interface

polymer	solid/water Σ_p [nm^2]	air/water[a] Σ_p [nm^2]	ratio
P123	2.25	0.50	4.5
P103	1.68	0.62	2.7
P104	2.45	0.77	3.2
P105	2.82	0.99	2.9
F108	5.69	1.52	3.7

[a] Data at $T = 25$ °C from Alexandridis et al.[1]

Given the poorer solubility and the more hydrophobic nature of middle PO block, we expect the polymers to adsorb on the surface with an anchor−buoy-type structure: the PO block forming a collapsed, relatively thin layer (the anchor) strongly adsorbed at the surface and the EO blocks forming the adjacent swollen layer (the buoy).

By comparing the size of a chain at the surface with the size of a free chain in the bulk solution, we can infer whether the polymers have adopted a flatter "mushroom" configuration or a more extended "brush" configuration. This can conveniently be done by looking at the values of the so-called reduced surface density σ^*, adjusted to keep into account the triblock structure of the polymer:[17]

$$\sigma^* = \frac{2\pi {R_g}^2}{\Sigma_p} \tag{1}$$

where R_g is the radius of gyration of a single EO chain in solution, having a number of segments equivalent to one buoy block, and Σ_p is the molecular area at the surface. It is thought that there are three regimes of stretching.[4] The first, for values of $\sigma^* \leq 2$, corresponds to the mushroom regime. The second, for values of $2 \leq \sigma^* \leq 20$, corresponds to a regime where the polymer forms a brush that progressively stretches away from the surface. Finally, in the third regime, $\sigma^* \geq 20$, the asymptotic limit is reached, and the chains in the brush are stretched out into the solution to the fullest extent possible. Combining the molecular area information from our experiments and radii of gyration data from the literature,[26] we estimate values of reduced surface coverages that range between 4, for the smallest sized polymer (P103, $E_{17}P_{60}E_{17}$), and 12, for the biggest sized polymer (F108, $E_{132}P_{50}E_{132}$). Thus, the expectation for our system is to exhibit behavior that is consistent with the existence of a brush at the surface.

We can analyze the adsorption amounts data in the context of the scaling theory of Marques, Joanny, and Leibler (MJL) for block copolymer adsorption from a selective solvent.[27] This theory applies to a copolymer that has an insoluble block with high affinity for the surface (the anchor) and a soluble block that does not adsorb (the buoy). MJL show that the thickness of the anchor layer d in equilibrium with a reservoir of polymer is obtained by minimizing the grand canonical free energy G with respect to the thickness at constant chemical potential μ_{ex} and constant osmotic pressure π_{ex}, where G is composed of four main terms:[31] a capillary energy, which represents the work necessary to replace a surface/solvent interface with surface/anchor and anchor/solvent interfaces, the chemical potential of the adsorbed chains in equilibrium with the reservoir, a van der Waals dispersion energy contribution to model the long-range interactions between the surface and the solvent mediated by the anchor layer, and finally the energy of the buoy layer. (The original MJL formulation has an additional term to account at very high surface concentrations of the stretching of the anchor layer; we neglect it as it does not apply to our system.) The density of the adsorbed chains σ is directly proportional to the anchor layer thickness d:

$$\sigma \sim d N_A \tag{2}$$

where N_A is the degree of polymerization of the anchor block.

Thus, minimization of the free energy (the constant capillary term drops out upon differentiation) yields the following expression:

$$\bar{\mu}_{ex} = -\alpha_{vdW} \frac{A}{T} {N_A}^{-2} \sigma^{-3} + \alpha_{brush} \beta^{5/3} {N_A}^{5/6} \sigma^{5/6} \tag{3}$$

where α_{vdW} and α_{brush} are positive numerical coefficients, A is the absolute value of the Hamaker constant, $\tilde{\mu}_{ex}$ is the effective chemical potential (as defined in MJL), and β is the so-called asymmetry ratio, the ratio between a solvated coil (buoy) and a characteristic Gaussian coil (anchor):

$$\beta = \frac{{N_B}^{3/5}}{{N_A}^{1/2}} a \tag{4}$$

where N_B and N_A are the degrees of polymerization of the buoy and the anchor blocks, respectively, and a is the ratio between buoy and anchor monomer sizes. Depending on the relative magnitude of the three terms in eq 3, we can have three characteristic regimes, named by MJL in the following way: the Rollin regime, the van der Waals−buoy regime, and the buoy-dominated regime. For an effective chemical potential that is negative and large, we are in the Rollin regime. The dominant term on the right-hand side is the van der Waals term, and the surface density does not depend on the buoy layer. As the absolute value of the effective chemical potential becomes small, we have the van der Waals−buoy regime. A balance between the van der Waals interactions and the stretching of the buoy layer determines the surface density. The range for this regime is given by the following limits:

$$-\left(\frac{A}{T} N_A\right)^{5/23} \beta^{30/23} < \tilde{\mu}_{ex} \leq \left(\frac{A}{T} N_A\right)^{5/23} \beta^{30/23} \tag{5}$$

For larger positive values of the effective chemical potential, we have the buoy-dominated regime, where the stretching energy of the buoy becomes the dominant term on the right-hand side of eq 3. This occurs for the following values of the effective chemical potential:

$$\tilde{\mu}_{ex} > \left(\frac{A}{T} N_A\right)^{5/23} \beta^{30/23} \tag{6}$$

The following scaling relations apply for the two regimes:

$$\text{van der Waals−buoy regime:} \quad \sigma \propto {N_B}^{-6/23} {N_A}^{-12/23} \tag{7}$$

$$\text{Buoy-dominated regime:} \quad \sigma \propto {N_B}^{-6/5} {N_A}^{12/25} \tag{8}$$

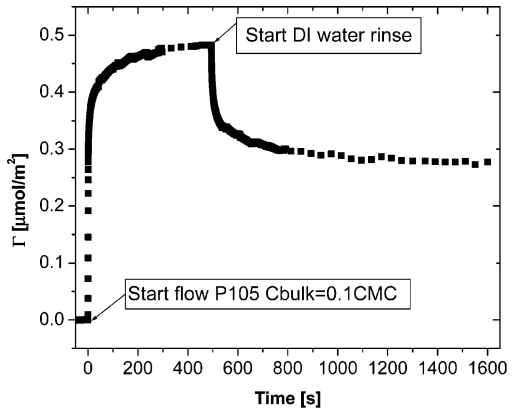

Figure 4. Typical adsorption−desorption kinetics experiment: a polymer residue is left on the surface after completing the rinsing step.

We have used best fits of eq 7 and eq 8 on the adsorbed amounts of the last two copolymers in the series (P105-($E_{37}P_{56}E_{37}$) and F108 ($E_{132}P_{50}E_{132}$)) to find the numerical coefficients of the correlations and then applied these functions for comparison with the experimental data for the remaining three copolymers. We compare the results of the fitting functions with the experimental data in Figure 3, where ν_A, the anchor fraction, is given by

$$\nu_A = \frac{N_A}{N_A + N_B} \tag{9}$$

In panel a we have the comparison for the series at (approximately) constant anchor block. The filled circles are the results of the fit for the buoy-dominated regime, and the filled triangles are the results of the fit for the van der Waals−buoy regime. The empty squares represent the experimental data points. We can see that the trends for this series are consistent with the buoy-dominated regime. The less than satisfactory match of the fit can be rationalized by recalling that the MJL model assumes no affinity of the buoy block segments for the surface. From past studies,[22,24] we know that the EO segments do have some affinity for the surface. Self-consistent mean-field calculations by Bijsterbosch et al.[5] have shown that the adsorbed amounts decrease as the affinity of the buoy block for the surface increases. They explained this in terms of the cost in translational and configurational entropy and the gain in energy for adsorbing a new anchor block in solution compared with the same for a buoy block of a chain that is already adsorbed. Panel b shows the same elements of the fit applied to the copolymer P123. In this case, we see that the buoy-dominated regime predicts higher adsorbed amounts than we find experimentally. The result is consistent with the van der Waals−buoy regime. This is not surprising since, even though P123 has an asymmetry ratio that is virtually the same as P103, this copolymer has a value of the cmc a factor of 6 smaller than that for P103, and thus we conclude that the value of the effective chemical potential for this copolymer lies below the limit that defines the transition between buoy-dominated and van der Waals−buoy regimes.

Desorption Isotherms. Figure 4 shows the outcome of a typical adsorption−desorption experiment. Adsorption of P105 is started at $t = 0$ s until $t = 500$ s.

At $t = 500$ s, the P105 is displaced by flowing distilled water. The polymer layer is not removed in its entirety upon rinsing with pure solvent; in fact, substantial residual amounts are left on the surface after very long rinsing times as shown in Figure 5.

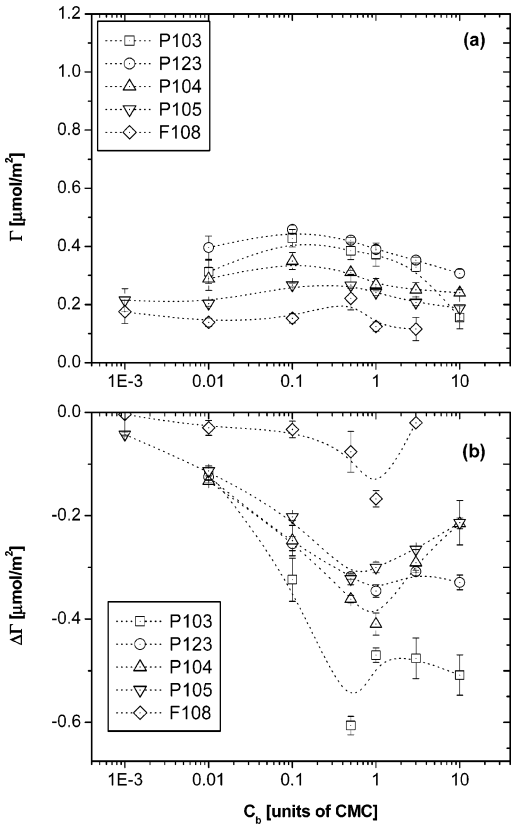

Figure 5. A log−linear graph of the desorption isotherms for Pluronics P103 ($E_{17}P_{60}E_{17}$), P123 ($E_{19}P_{69}E_{19}$), P104 ($E_{27}P_{61}E_{27}$), P105 ($E_{37}P_{56}E_{37}$), and F108 ($E_{132}P_{50}E_{132}$): (a) residual amount left on surface at end of desorption experiment; (b) absolute change in surface excess concentration (residual minus adsorbed amount at start of desorption experiment).

Figure 5 shows desorption in terms of the amount left on the surface (a) and the amount desorbed (b). A possible explanation for the incomplete desorption is that the large number of segments adsorbed collectively create a large energy barrier, hindering the simultaneous breakage of all segment−surface contacts and hence precluding desorption.[7] The observed partial desorption would then likely be due to the fact that, while the PPO segments with the higher affinity for the hydrophobic surface constitute the bulk of the irreversible surface contacts, a fraction of these contacts may be ascribed to the more labile PEO segments. Another possibility is that the adsorbed layer is in fact fully equilibrated with the solution adjacent to the interface, but because of the high-affinity character of the isotherms, it would take only a small amount to desorb for the concentration near the interface to drop to a very small level, making the process quickly mass-transport limited with a very small driving force.[14,15,21]

Atomic Force Microscopy. We have employed soft contact imaging AFM[32] to resolve the morphology of P103 ($E_{17}P_{60}E_{17}$) and P105 ($E_{37}P_{56}E_{37}$) systems at or above the cmc. Soft contact imaging consists of exercising a delicate balance between imposing a sufficient amount of force on the probing tip, so that a good contrast in the image is achieved, and ensuring that the integrity of the substrate is not compromised. In Figure 6 we show micrographs obtained for P105 at the cmc.

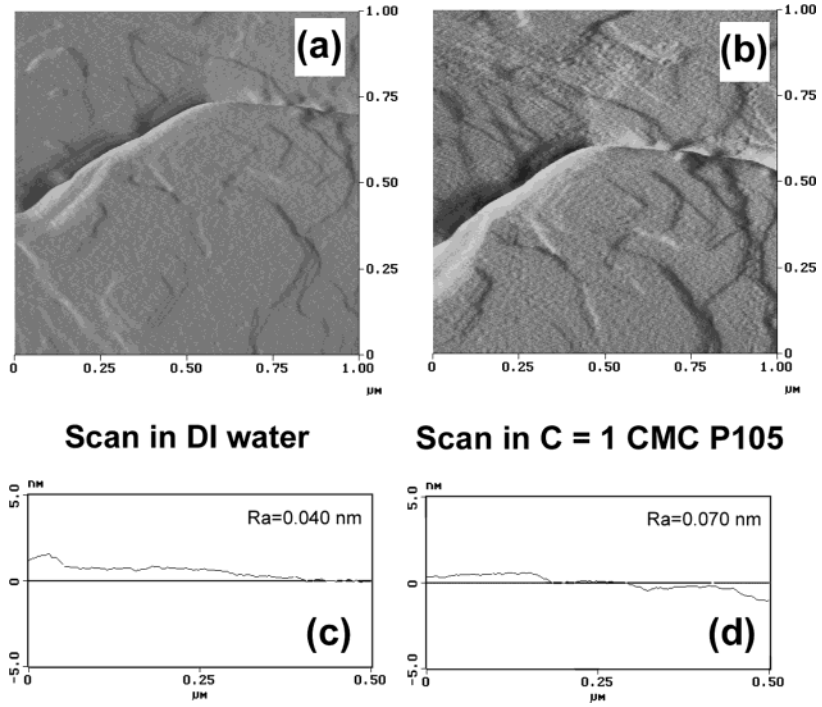

Figure 6. Atomic force microscopy scans in solution for P105 ($E_{37}P_{56}E_{37}$). (a) Scan prior to exposure to the polymer solution; (b) scan in $C = 1$ cmc P105 solution; (c) and (d) representative sections for the two respective scans.

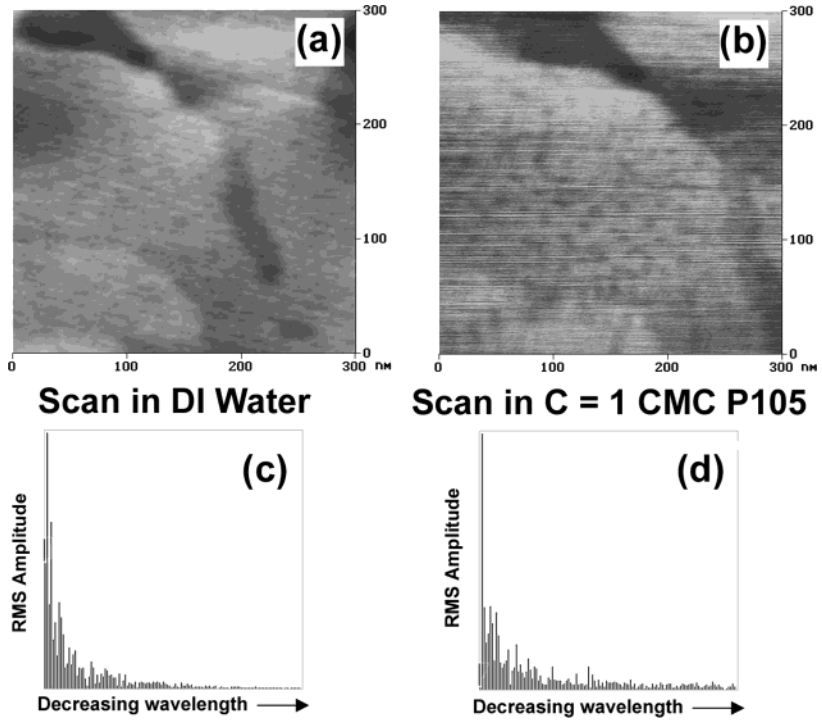

Figure 7. Magnified views of the AFM scans in Figure 6: (a) scan prior to exposure to the polymer solution; (b) scan in $C = 1$ cmc P105 ($E_{37}P_{56}E_{37}$) solution; (c) and (d) fast Fourier transform spectra for characteristic sections of the two scans.

Panel a is the control, that is, the bare undecanethiol substrate in DI water; panel b is the image of the surface after exposure to the P105 solution; and panels c and d show, for the respective images, a typical section along with a characteristic value for the average roughness. Figure 6b shows a change of texture although there is barely any change in the roughness values. Figure 7 shows a higher resolution version of the same images that highlight the change in texture; in addition, the fast Fourier transform spectra in panels c and d show that there is a net increase in roughness at the nanoscale frequencies.

The combination of the two images point to the creation of a smooth adsorbed layer. Similar results are obtained at 10 cmc, where, again, we observe a very compact and smooth layer for P105 (Figure 8).

On the other hand, when we look at P103, we find a completely different type of morphology at the surface. Figures 9 and 10 show the results for surfaces exposed respectively to 1 cmc and 10 cmc P103 solutions. We

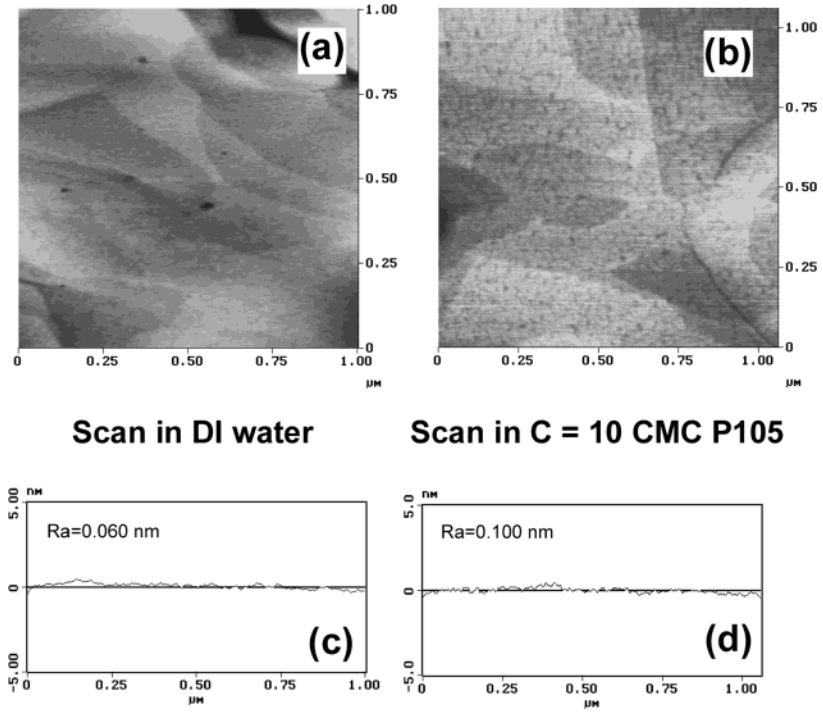

Figure 8. Atomic force microscopy scans in solution for P105 ($E_{37}P_{56}E_{37}$): (a) scan prior to exposure to the polymer solution; (b) scan in $C = 10$ cmc P105 solution; (c) and (d) representative sections for the two respective scans.

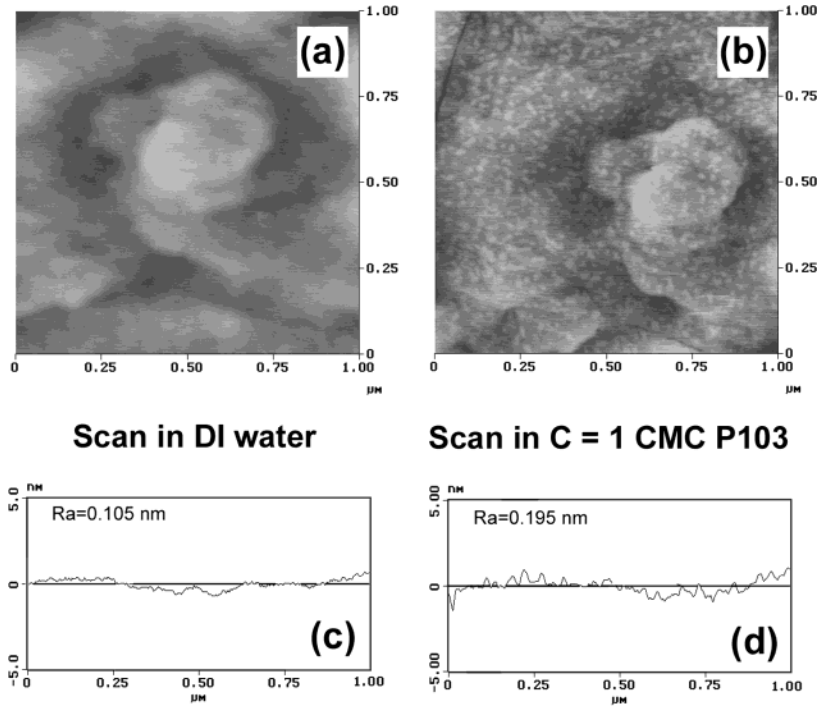

Figure 9. Atomic force microscopy scans in solution for P103 ($E_{17}P_{60}E_{17}$): (a) scan prior to exposure to the polymer solution; (b) scan in $C = 1$ cmc P103 solution; (c) and (d) representative sections for the two respective scans.

see the appearance of very distinct, globular-type surface aggregates at both concentrations. The apparent dimensions (tip convolution effects may play a role[37]) are given on top of the section in Figure 11. As seen in Figure 11, the vertical dimension of the aggregate is about 1 nm and the lateral dimension is about 30 nm. These values compare with a value of about 5 nm for the diameter of the PPO core of a micelle in solution[39] and a value of about 20 nm for the hydrodynamic diameter of the whole micelle in solution.[30] To get a better feel for the observed dimensions on surfaces, we need to discuss the conditions used to capture the previous images. Figure 12 shows a deflection vs probing tip distance from the surface, what is known as a force plot. (Deflections can be converted to forces if an accurate value for the cantilever constant is available.)

From Figure 12 we see that when the tip is about 34 nm away from the surface, it begins to undergo steric interactions with the polymer film; most likely, the tip first comes into contact with the softer PEO brush. As the applied force is increased, the repulsion sharply increases until the film yields and the tip jumps to make

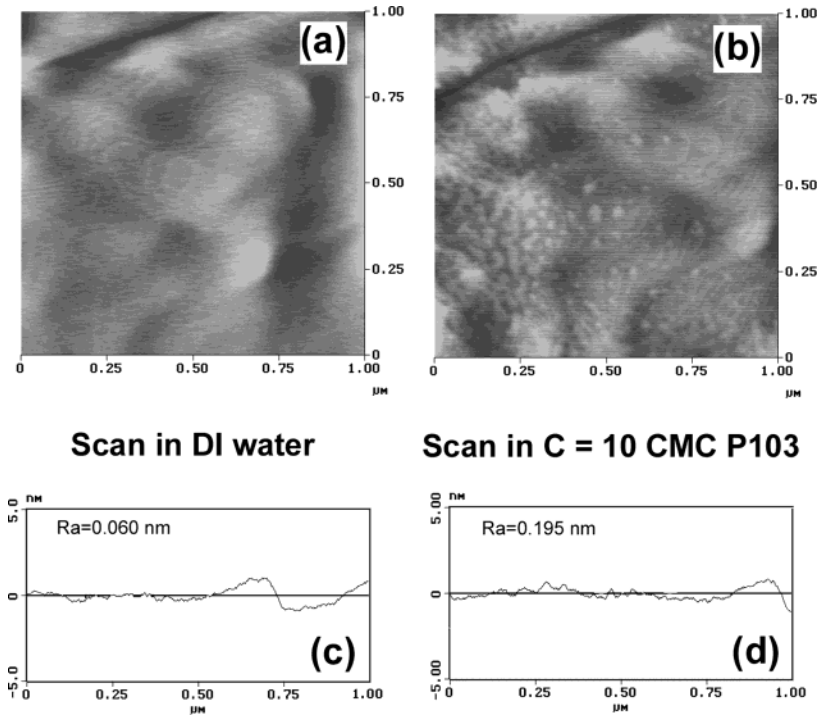

Figure 10. Atomic force microscopy scans in solution for P103 ($E_{17}P_{60}E_{17}$): (a) scan prior to exposure to the polymer solution; (b) scan in $C = 10$ cmc P103 solution; (c) and (d) representative sections for the two respective scans.

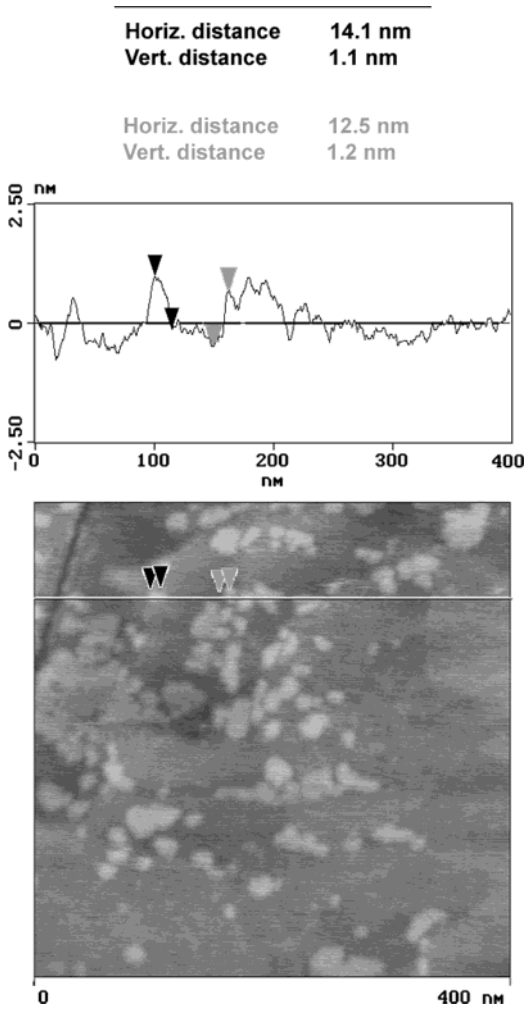

Figure 11. Magnified views of the AFM scan in Figure 9 and representative section. The numbers at the top of the figure give the apparent dimensions of two individual aggregates.

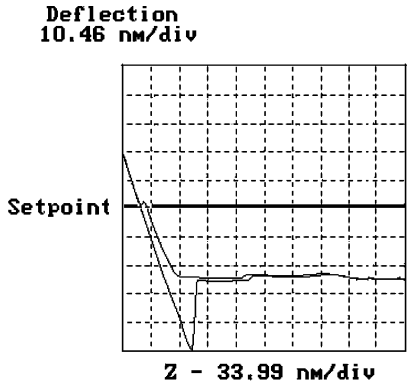

Figure 12. Typical AFM tip force−plot response for the P103 ($E_{17}P_{60}E_{17}$) polymer system: distance of AFM tip from the surface on the *x*-axis; cantilever deflection on *y*-axis.

hard contact. Generally, in capturing the images, we have operated at a set point that is close to the jump-off condition, and thus we expect that the features shown in Figure 11 correspond to the layer's PPO inner core. In fact, if we relax the applied load, we see the emergence of completely different features. Figure 13 shows the behavior for a P105-coated surface when the force is cycled between a higher and a lower setting.

Likewise, Figure 14 shows the behavior for a P103-coated surface. When the applied load is low, diffuse globules appear for both polymer surfaces. A close examination of the pairs of images (a) and (b) as well as (c) and (d) in Figure 14 reveals that the surface micellar aggregates are stationary; they are not being displaced by the tip. The lower force images corroborate the results of our previous analysis for the presence of an outstretched PEO polymer brush dangling in the solution. The higher force scans, instead, represent the imaging of PPO inner cores. With the latter considerations in mind, and the relative dimensions of the adsorbed PEO brushes and PPO cores, we can conclude

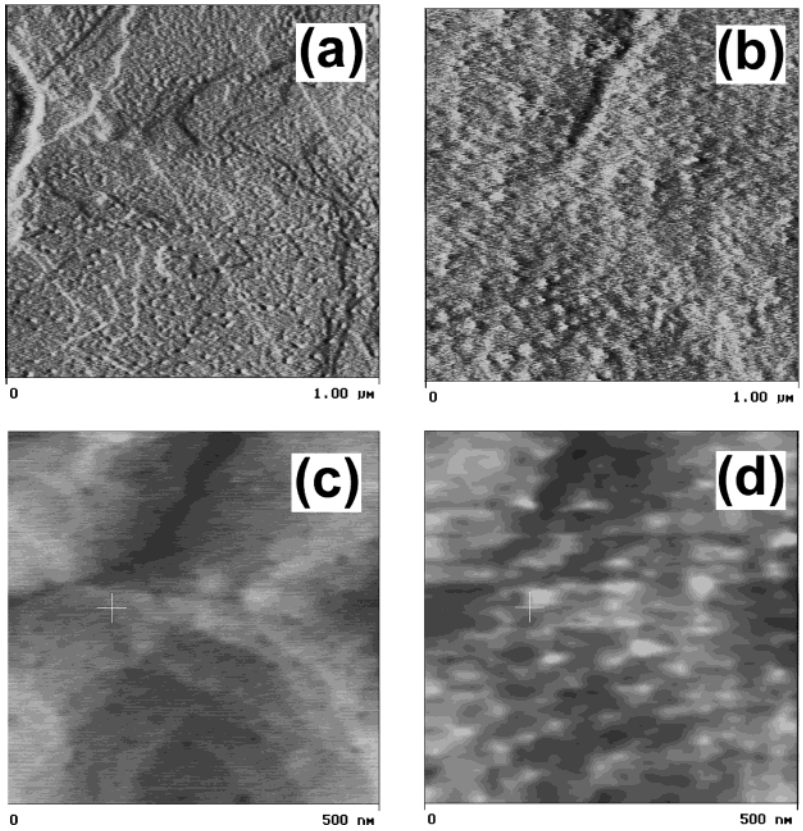

Figure 13. Atomic force microscopy images (same area) of a P105 ($E_{37}P_{56}E_{37}$)-coated surface. Cycling between high and low values of the force applied to the AFM tip. (a, c) Scans with higher force setting; (b, d) scans with lower force setting. (a) and (b) are 1 μm $\times$ 1 μm scans; (c) and (d) are 500 nm $\times$ 500 nm scans of the same area.

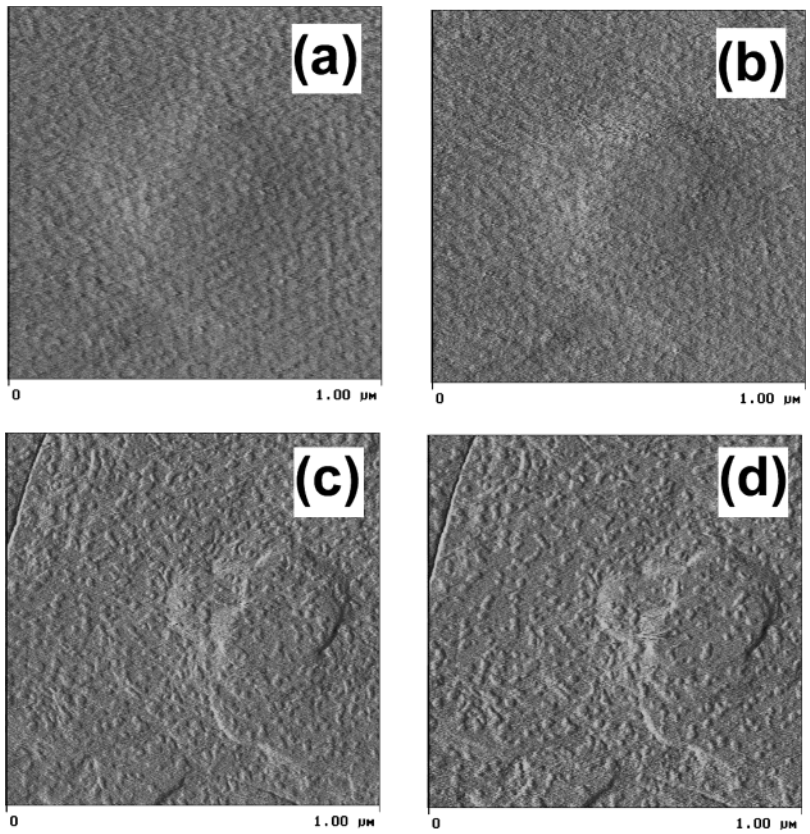

Figure 14. Atomic force microscopy images of P103 ($E_{17}P_{60}E_{17}$)-coated surface. Sequence of low to high values of the force applied to the AFM tip. All images are taken at the same location. (a, b, c, d) Scans with progressively higher force settings.

that the shape and dimensions of the micelles in solution are closely related in size to the aggregates at the surface except that the PPO core assumes a more planar configuration by wetting the surface. Similar

observations have been reported for other triblock copolymer systems.[16,38,40]

Conclusions

We have investigated the adsorption and desorption of behavior of a family of triblock copolymers on model hydrophobic surfaces. This study shows that the adsorbed amounts are not consistent with the Langmuir isotherm and that the adsorption process is only partially reversible. Scaling law analysis shows that the copolymers with increasing size of the hydrophilic block are in the buoy-dominated regime. A transition to the van der Waals−buoy regime is observed for the copolymer with the largest size of the hydrophobic block. AFM imaging reveals the presence of micellar-like aggregates at the surface for the copolymer with higher relative hydrophobic content (P103) and a uniform morphology for a copolymer with higher hydrophilic content (P105). In both cases, cycling of the force on the AFM tip reveals the presence of a polymer brush.

Acknowledgment. The National Science Foundation (NSF) under Award DMR-9808677 funded this work. P. Brandani acknowledges additional support through a NSF fellowship from the NEAT-IGERT program (IGERT Grant DGE-9972741).

References and Notes

(1) Alexandridis, P.; Athanassiou, V.; Fukuda, S.; Hatton, T. A. *Langmuir* **1994**, *10*, 2604−2612.
(2) Alexandridis, P.; Holzwarth, J. F.; Hatton, T. A. *Macromolecules* **1994**, *27*, 2414−2425.
(3) Amiji, M. M.; Park, K. *J. Appl. Polym. Sci.* **1994**, *52*, 539−544.
(4) Baranowski, R.; Whitmore, M. D. *J. Chem. Phys.* **1995**, *103*, 2343−2353.
(5) Bijsterbosch, H. D.; Cohen Stuart, M. A.; Fleer, G. J.; van Caeter, P.; Goethals, E. J. *Macromolecules* **1998**, *31*, 7436−7444.
(6) Born, M. *Principles of Optics*, 6th ed.; Pergamon Press: Oxford, 1980; p 58.
(7) Braem, A. D.; Prieve, D. C.; Tilton, R. D. *Langmuir* **2001**, *17*, 883−890.
(8) Bunjes, N.; Schmidt, E. K.; Jonczyk, A.; Rippmann, F.; Beyer, D.; Ringsdorf, H.; Graber, P.; Knoll, W.; Naumann, R. *Langmuir* **1997**, *13*, 6188−6194.
(9) Chakraborty, A. K.; Golumbfskie, A. J. *Annu. Rev. Phys. Chem.* **2001**, *52*, 537−573.
(10) Cohen-Stuart, M. A. Macromolecular Adsorption: A Brief Introduction. In *Biopolymers at Interfaces*; Malmsten, M., Ed.; Marcel Dekker: New York, 1998; Vol. 75, pp 1−25.
(11) Creager, S. E.; Clarke, J. *Langmuir* **1994**, *10*, 3675−3683.
(12) De Feijter, J. A.; Benjamins, J.; Veer, F. A. *Biopolymers* **1978**, *17*, 1759−1772.
(13) Debruijn, H. E.; Altenburg, B. S. F.; Kooyman, R. P. H.; Greve, J. *Opt. Commun.* **1991**, *82*, 425−432.
(14) Dijt, J. C.; Cohen Stuart, M. A.; Fleer, G. J. *Macromolecules* **1992**, *25*, 5416−5423.
(15) Dijt, J. C.; Cohen Stuart, M. A.; Fleer, G. J. *Macromolecules* **1994**, *27*, 3207−3218.
(16) Eskilsson, K.; Grant, L. M.; Hansson, P.; Tiberg, F. *Langmuir* **1999**, *15*, 5150−5157.
(17) Eskilsson, K.; Tiberg, F. *Macromolecules* **1997**, *30*, 6323−6332.
(18) Eskilsson, K.; Tiberg, F. *Macromolecules* **1998**, *31*, 5075−5083.
(19) Green, R. J.; Tasker, S.; Davies, J.; Davies, M. C.; Roberts, C. J.; Tendler, S. J. B. *Langmuir* **1997**, *13*, 6510−6515.
(20) Hansen, W. N. *J. Opt. Soc. Am.* **1968**, *58*, 380.
(21) Huang, Y.; Santore, M. M. *Langmuir* **2002**, *18*, 2158−2165.
(22) Huang, Y. W.; Gupta, V. K. *Macromolecules* **2001**, *34*, 3757−3764.
(23) Kayes, J. B.; Rawlins, D. A. *Colloid Polym. Sci.* **1979**, *257*, 622.
(24) Kelly, M. S.; Santore, M. M. *Colloids Surf., A* **1995**, *96*, 199−215.
(25) Knoll, W. *Annu. Rev. Phys. Chem.* **1998**, *49*, 569−638.
(26) Li, J. T.; Caldwell, K. D.; Rapoport, N. *Langmuir* **1994**, *10*, 4475−4482.
(27) Marques, C.; Joanny, J. F.; Leibler, L. *Macromolecules* **1988**, *21*, 1051−1059.
(28) Munch, M. R.; Gast, A. P. *J. Chem. Soc., Faraday Trans.* **1990**, *86*, 1341−1348.
(29) Muthukumar, M.; Ober, C. K.; Thomas, E. L. *Science* **1997**, *277*, 1225−1232.
(30) Nolan, S. L.; Phillips, R. J.; Cotts, P. M.; Dungan, S. R. *J. Colloid Interface Sci.* **1997**, *191*, 291−302.
(31) Parsonage, E.; Tirrell, M.; Watanabe, H.; Nuzzo, R. G. *Macromolecules* **1991**, *24*, 1987−1995.
(32) Patrick, H. N.; Warr, G. G.; Manne, S.; Aksay, I. A. *Langmuir* **1997**, *13*, 4349−4356.
(33) Peppas, N. A.; Langer, R. *Science* **1994**, *263*, 1715−1720.
(34) Peterlinz, K. A.; Georgiadis, R. *Langmuir* **1996**, *12*, 4731−4740.
(35) Peterlinz, K. A.; Georgiadis, R. *Opt. Commun.* **1996**, *130*, 260−266.
(36) Tiberg, F.; Landgren, M. *Langmuir* **1993**, *9*, 927−932.
(37) Koutsos, V. Ph.D. Dissertation, Rijksuniversiteit, Groningen, 1997.
(38) Marsh, L. H.; Coke, M.; Dettmar, P. W.; Ewen, R. J.; Havler, M.; Nevell, T. G.; Smart, J. D.; Smith, J. R.; Timmins, B.; Tsibouklis, J.; Alexander, C. *J. Biomed. Mater. Res.* **2002**, *61*, 641.
(39) Mortensen, K.; Pedersen, J. S. *Macromolecules* **1993**, *26*, 805.
(40) Wu, C. H.; Liu, T. B.; White, H.; Chu, B. *Langmuir* **2000**, *16*, 656.

MA0342675